Catena 269 (2026) 110032

Contents lists available at ScienceDirect

Catena

journal homepage: www.elsevier.com/locate/catena

A new cryptic Refugium: the Gran Zebrù Nunatak (2900 m asl) during the last glacial maximum in the European Central Alps

Mauro Guglielmin [a,b,*], Alessandro Longhi [a,b], Eleonora Balliana [c], Roberta Bettinetti [d,b], Carlotta Santolini [d,e], Dario Battistel [c]

[a] Department of Theoretical and Applied Sciences, Insubria University, Varese, Via J.H. Dunant, 3, 21100, Italy
[b] Climate Change Research Center, Insubria University, Varese, Via J.H.Dunant, 3, 21100, Italy
[c] Department of Environmental Sciences, Informatics and Statistics, Ca' Foscari University, Venezia Mestre, Via Torino, 155, 30170, Italy
[d] Department of Human Sciences and Innovation for the Territory, Insubria University, Como, Via Valleggio 11, 22100, Italy
[e] University School for Advanced Studies IUSS, Pavia, Italy

ARTICLE INFO

Dataset link: PC2values (Original data)

Keywords:
Last glacial maximum
Nunatak
Climate change
Paleolimnology
XRF
Diatoms
Macroremains

ABSTRACT

In this paper, we present the finding of a new cryptic refugium in the Central European Alps at 2900 m asl, revealed through multiproxy analyses of paleolacustrine sediments at the foot of Gran Zebrù peak. The sediment core revealed the presence of a paleolake from ca 30,000 cal BP until 18,500 cal BP, when a hiatus in sedimentation occurred, followed by an intense weathering phase lasting until 13,700 cal BP. Lake sedimentation then restarted and continued until 9000 cal BP. Throughout this interval, glaciers surrounded the nunatak and flowed into the valleys, as also occurred during at least three subsequent periods (13,700-13,000, 11,500–11,000 and 10,000–9600 cal BP.), when the presence of trees, and therefore of a cryptic refugium, was demonstrated by plant macroremains. Since at least 26,700 cal BP, these climatic phases were also recorded by the second principal component (PC2) of the sediment geochemistry, which explains approximately 20% of the total variance. PC2 is characterized by a strong positive loading of Ca/Ti (0.921) and a weaker negative loading of Si/Ti (−0.364), which closely mirror the temperature reconstructions based on Greenland ice cores.

1. Introduction

The Pleistocene glacial evolution of the European Alps is still debated, especially in their interior regions, where different glaciations may overlap or be indistinguishable (Kelly et al., 2004). The evolution of the glacier extent in this part of the mountain chain is not well constrain (Longhi et al., 2020). However, according to the glacial map of Ehlers et al., 2011, not shown) several peaks in the Italian central alps protruded above the ice cover and may have functioned as nunataks.

The term *nunatak* was introduced since 1877 to describe a mountain peak or ridge that protrudes through the surface of an ice sheet or glacier. Only a few years later, Blytt (1882) proposed his "nunatak theory", identifying these areas as sites of in situ glacial survival for various living organisms (e.g. plants and mammals), which could subsequently act as sources for their rapid expansion into newly ice-free areas, thus acting as "biological refugia".

Since then, many studies have been carried out both to identify such areas and to investigate their characteristics (e.g. Ballantyne, 1998; Birks, 1994; Birks and Willis, 2008; Carcaillet and Blarquez, 2017; Carcaillet et al., 2018; Goodfellow, 2007; Kullman, 2008; McCarroll et al., 1995; Öberg and Kullman, 2011; Parducci et al., 2012; Schönswetter et al., 2005) as well as to analyze the mechanism involved and to classify different type of refugia (e.g. Brochmann et al., 2003; Holderegger and Thiel-Egenter, 2008; Rull, 2008; Stewart et al., 2010).

Only a limited number of these studies have focused on the European Alps (Carcaillet and Blarquez, 2017; Carcaillet et al., 2018; Schönswetter et al., 2005;) and, to the best of our knowledge, only one has been conducted at high elevation on the Italian Alps (Pintaldi et al., 2021). Among the different types of refugia described by Holderegger and Thiel-Egenter (2008), nunatak refugia may provide spatially limited patches of suitable habitat, acting as the microrefugia sensu Rull (2008) such steep, south-facing slopes of high summits during glaciations (see Fig. 1, p. 477 in Holderegger and Thiel-Egenter, 2008).

These microrefugia comprise areas with sheltered topography and buffered, stable local microclimates (Stewart and Lister, 2001), characterized by exceptional physiography (e.g. warm soils or freshwater

* Corresponding author at: Department of Theoretical and Applied Sciences, Insubria University, Varese, Via J.H. Dunant, 3, 21100, Italy.
E-mail address: mauro.guglielmin@uninsubria.it (M. Guglielmin).

https://doi.org/10.1016/j.catena.2026.110032
Received 8 August 2025; Received in revised form 5 March 2026; Accepted 19 March 2026
Available online 17 April 2026

springs), and well exposed to sun light (high solar irradiance). Together, these conditions favor the biogeochemical processes required for tree growth and their associated biota.

In some cases, nunatak can host lakes or paleolake, whose sediments archive paleoclimatic information and give the opportunity to constrain the timing of deglaciation in these areas (i.e. Carcaillet and Blarquez, 2017; Gjærevoll, 1963; Paus, 2010; Paus et al., 2011).

Paleolacustrine sediments have become increasingly important for the study of long-term environmental change due to their ability to provide high-resolution records of past conditions. The last 30,000 years have been marked by significant climatic variations, including the Last Glacial Maximum (LGM), the termination of the LGM, and the Holocene (Alley et al., 2010). These climatic fluctuations significantly affected the environment, leading to changes in vegetation patterns, lake levels, and sedimentation rates.

The use of multiproxies in the analysis of paleolacustrine and other sedimentary archives has substantially improved the understanding of past environmental changes. Grain size variations have been widely used to detect changes in depositional energy related to wetter and dryer periods (Schmidt et al., 2006). Similarly, organic matter (OM) has been widely used in paleoenvironmental studies to infer changes in vegetation, lake productivity, and temperature (Heiri et al., 2001).

Pigment analyses provide insights into changes in primary productivity.

over time and has been used to reconstruct past environmental conditions, as well as to assess the potential occurrence of eutrophication and acidification processes (Jiménez et al., 2015). Another widely applied approach is plant macroremains analysis, which allows the reconstruction of past environmental changes, including shifts in vegetation cover and lake level fluctuations (Blaauw et al., 2007; Meeks et al., 2017).

Diatom analysis has been extensively in paleolacustrine sediment studies. Diatoms provide valuable information on past water chemistry, such as pH and nutrient availability, and they can be used to infer

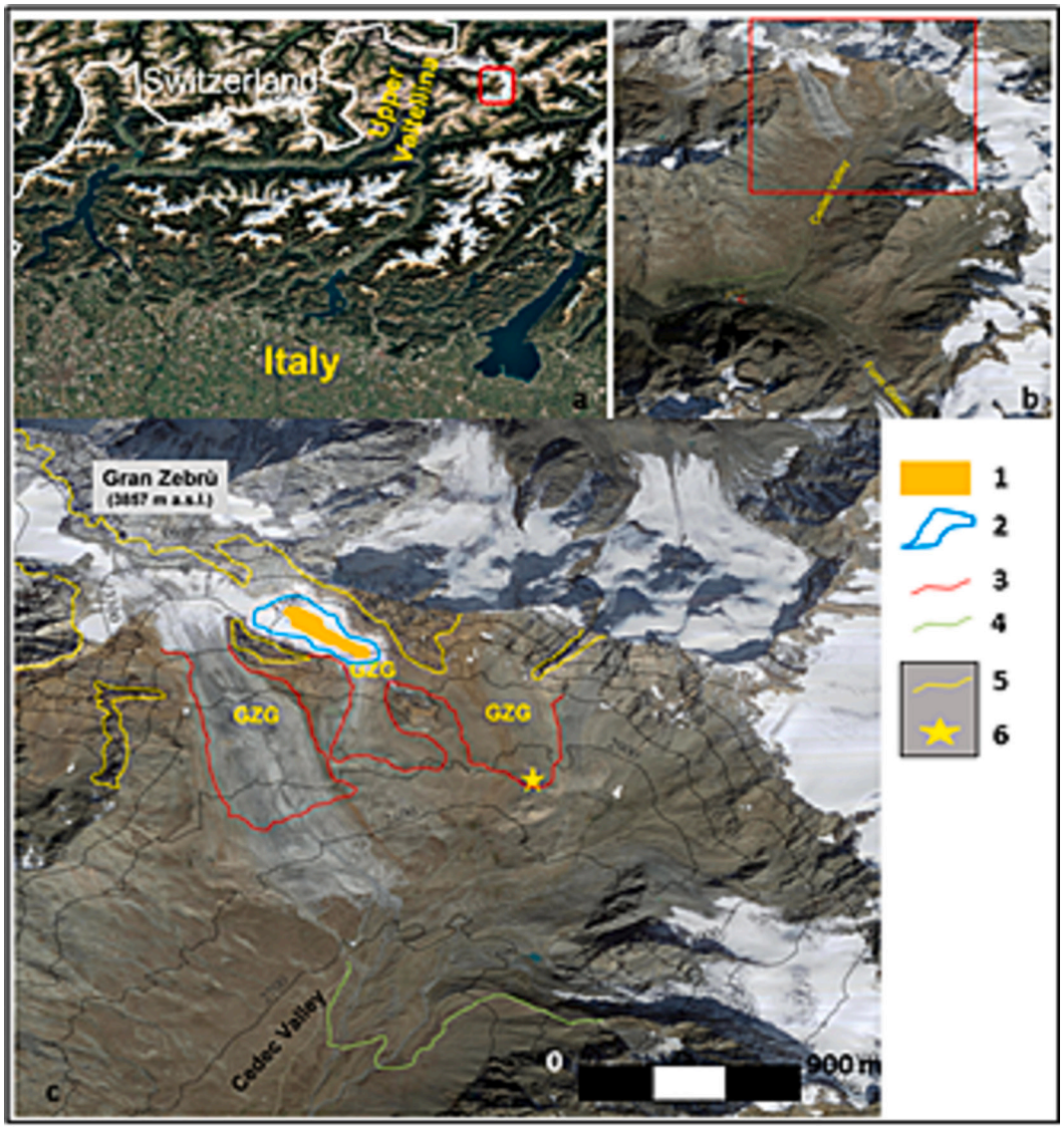

Fig. 1. The study area in the Central European Alps (a); b) detail of the Cedec Valley and Forni Glacier areas where are shown the Late Glacial and Early Holocene glacial advances (green line = 15,000; orange line = 11,800 and red line 9700 Cal BP years (Longhi and Guglielmin, 2021 redrawn); c) upper cedec Valley, Gran Zebrù (3949 m asl) and GZG area. Legend: 1) body of frozen debris below the GZG (Forte et al., 2021), 2) GZG limit on 2021 CE; 3) GZG limit at 1931 CE; 4) GZG limit at Little Ice Age; 5) Trimline; 6) our paleolacustrine core. The basemap for the panel a is Google – Maxar Technologies 2025 and for panels b and c from is ortophoto AGEA 2018 (from Geoportale Regione Lombardia). (For interpretation of the references to colour in this figure legend, the reader is referred to the web version of this article.)

environmental changes including variations in lake level, temperature and ice cover dynamics (Battarbee et al., 2001; Rühland et al., 2015;).

Among the chemical proxies X-ray fluorescence (XRF) analysis is commonly applied to determine elemental composition and to infer past environmental processes, such as changes in erosion rates, sediment sources, and atmospheric deposition (Biskaborn et al., 2012; Cartier et al., 2018; Vyse et al., 2020). In particular, some of these proxies, such as plants macroremains and charcoal, can indicate whether surrounding areas provided suitable conditions for biological refugia, as demonstrated, for example, by Carcaillet and Blarquez (2017).

This work aims to demonstrate, through the multiproxy analyses, that even in the interior part of the Alps at high elevation, within areas characterized by substantial ice accumulation, not only rocky peaks protruded above the ice, but also some ice-free slopes could persist. Specifically, we found that areas around 3000 m asl at the foot of Gran Zebrù peak, may have served as nunatak refugia and biodiversity hotspots, favouring an ecological connection between the two sides of the Alps.

2. Study area

The study area is located in the upper part of the Val Cedèc (Fig. 1) a north-south glacial valley located in the Central Italian Alps. The upper part of the valley was covered by the Gran Zebrù Glacier (GZG) during the Little Ice Age (LIA) up to 1872 CE (Pelfini, 1992), except over the trimline that is detectable on the rock cliffs between 3050 and 3150 m asl. The flat area, where the paleolacustrine sediments analysed were found, was abandoned by the LIA GZG around 1952 CE. The paleolake is roughly quadrangular (~ 70 m × 60 m) and occupies an area of more than 4000 m^2. It is difficult to precisely define the extent of the nunatak refugium due to the high slope dynamics. However, the occurrence of paleosols (podzols older than 14,000 cal BP, Longhi and Guglielmin, unpublished results) in nearby areas (less than 300 m, see Fig. 2) together with the presence of pebbles and rock outcrops showing well-developed weathering rinds and, in some cases, also varnish provides indirect evidence of prolonged ice-free conditions.

A tentative reconstruction of the refugium extent around 15,000 cal BP is reported in Fig. 2. The area is characterized by south-facing slopes, as well as terraces and small depressions surrounding the investigated paleolake at the foot of the rock cliffs, reaching elevation of approximately ~2750 m asl. The geology of the area is quite complex because different rock types are present, including sedimentary limestones (Calcare di Quattervals), magmatic bodies (Gran Zebrù pluton), and metamorphic rocks (Deichmann et al., 2012).

Recent climatic record achieved during the Glacier CC project funded by Stelvio National Park indicated that the mean annual air temperature is around −2 °C with the mean summer (JJA) air temperature exceeding 4 °C in 2020 and a total snow accumulation of only 0.2 m of water equivalent (Tarca and Guglielmin, 2022).

3. Methods

3.1. Coring, field description, and subsampling

In the deepest part of a paleolake (Fig. 2), following the current surface morphology, and at an elevation of 2950 m a.s.l., a 1.05 m sediment core was sampled using an Eijkelkamp piston sampler 01.09. The core was then described reporting texture and colour differences using the Munsell colour chart. The core segments were then sealed in aluminum foil and kept frozen at −20 °C.

Once in the lab, the core was sewed in 4 parts: one of these parts was kept untouched for XRF analysis, while from each of the other three faces a sample was extracted using a 1 cm^3 standard sampler for further analysis. All the laboratory analyses were performed only in the finer units below the depth of 45 cm.

3.2. Radiocarbon dating

Four samples were collected at different depths from key points of interest within the core, sealed in aluminum foil, and frozen at −20 °C. The samples were kept frozen until being sent to Beta Analytic Laboratories for radiocarbon dating. Respectively TBC-A at the beginning of the lacustrine sediments 46/48 cm, TBC-B at 79/81 cm, TBC-C at 89/91 cm, and TBC-D at 103/105 cm (the bottom of the lacustrine deposits). All conventional radiocarbon ages (CRA) were calibrated against the IntCal20 Northern Hemisphere calibration curve (Reimer et al., 2020) using the CLAM package. The subsequent age-depth model was generated with CLAM (version 2.6.2, Blaauw, 2010) using a linear accumulation model, accounting for the hiatus at 84–88 cm (see Fig. 3). Radiocarbon ages are reported as conventional radiocarbon years BP (^{14}C yr BP) and as calibrated age ranges with a 2σ error (95.4%) (cal. yr BP; relative to 1950 CE). To better evaluate the validity of the bulk sediment dating, $\delta^{13}C$ (Keith and Weber, 1964; Aitken, 1990) was calculated separately from the AMS carbon dating with IRMS by Beta

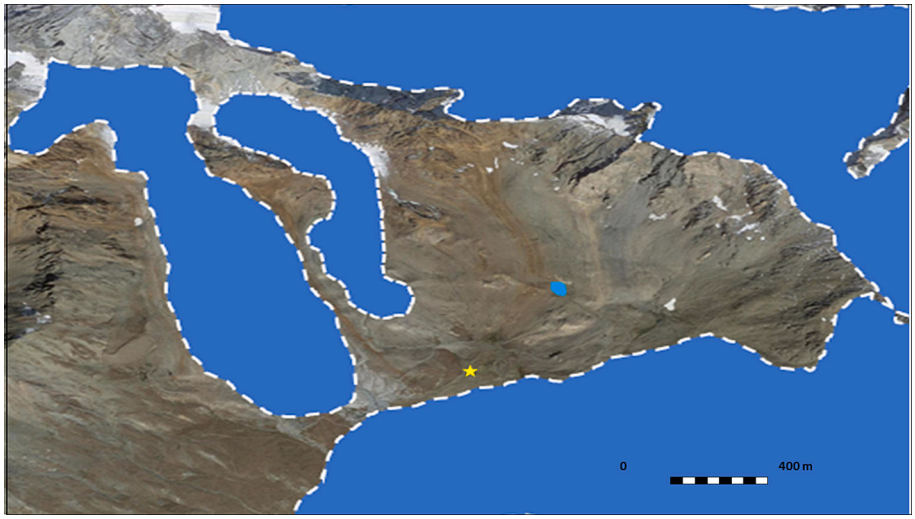

Fig. 2. Reconstruction of the GZN around 15,000 cal BP. In turquoise the extension of the lake while the yellow star indicates the paleopodsol dated around 15,000 cal BP. Glaciers are in blue with the white-dashed borders. (For interpretation of the references to colour in this figure legend, the reader is referred to the web version of this article.)

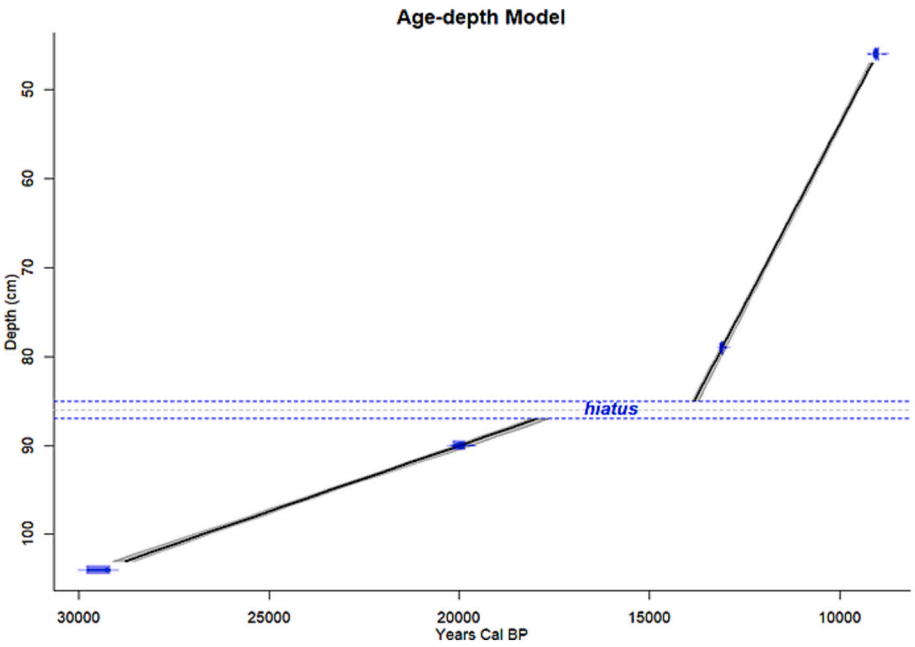

Fig. 3. Linear accumulation age-depth model accounting for the interruption of sedimentation (hiatus, dashed blue lines) after the deposition of the gravelly layer between 88 and 84 cm. (For interpretation of the references to colour in this figure legend, the reader is referred to the web version of this article.)

Analytic Laboratories.

3.3. Sediment analyses

The grain size distribution was measured merging 2/3 adjacent and dried 1cm^3 samples in order to have enough material and using a series of sieves with varying mesh sizes (25 mm, 12.5 mm, 9.5 mm, 6.3 mm, 4.7 mm, 2.36 mm, 2 mm, 1.18 mm, 0.6 mm, 0.425 mm, 0.3 mm, 0.18 mm, 0.15 mm, 0.106 mm, and 0.075 mm), and then classified according to the ASTM classification (ASTM, 2007).

The organic matter (OM) was estimated using the method of the Loss Of Ignition (LOI) as well as the carbonates.

Indeed, the LOI method is widely used in sediment analysis to estimate both organic and inorganic components, such as carbonates (Heiri et al., 2001). During heating, the organic and the carbonates components in the sample decomposed, releasing carbon dioxide and causing weight loss that can be measured to determine the carbonate content and organic carbon content (Nelson and Sommers, 1996). The samples are dried at 100 °C before being weighed and placed in a crucible for heating. The heating should be carried out in a muffle furnace at first temperature of 400 °C for organic carbon and 900 °C for carbonates (Heiri et al., 2001). Additionally, it is important to ensure that the sample is well-mixed and homogeneous, as variations in carbonate content and organic carbon across the sample can affect the accuracy of the LOI measurement. The OM is then calculated with the equation:

$$OM = \left(\frac{W_{100°C} - W_{400°C}}{W_{100°C}}\right) \times 100$$

Where $W_{400°c}$ represents the weight of the sediment samples after the 400 °C heating while $W_{100°c}$ is the weight of the soil after the 100°C drying.

The Inorganic Carbon (IC) is finally calculated with the equation:

$$IC = \left(\frac{W_{400°C} - W_{900°c}}{W_{400°C}}\right) \times 100$$

where $W_{900°c}$ represents the weight of the soil sample after the 900 °C heating.

3.4. Clorophyll (CD) and total carotenoids (TC)

One sample (1 cm^3) every 3 cm was then treated for algal and bacterial pigments extractions. The sample was soaked in a 90:10 solution of acetone (4.5 ml) and distilled water (0.5 ml) in a nitrogen atmosphere for 18 h following Lami et al. (2000). The extract was then centrifuged at 5000 rpm for 10 min, filtered, and 1 ml of acetone was added. This wash was carried out for two times. The extracts were then preserved in the dark to avoid photo-oxidation and then analysed using a spectrophotometer for total content in chlorophyll derivates (Adams et al., 1978) and total carotenoids content (Lami et al., 1994) at 450 nm and 665 nm, respectively. The concentrations of chlorophyll derivatives (CD) and total carotenoids (TC) were respectively calculated as in Guilizzoni et al. (1992) and Züllig (1982).

3.5. Macroremains

One sample of 1cm^3 every 3 cm was then dried and sieved to remove eventually large debris. The sediment was then washed, as macroremains usually float at the surface of the water (Jackson and Lyford, 1999). Macroremains were then hand-picked under a microscope and identified to the lowest possible taxonomic level using reference books and images (Jones, 1991; Van Geel et al., 1996; Pearsall, 2000). Finally, macroremains abundance was counted and recorded.

3.6. Diatoms

One sample (1 cm^3) every 3 cm was finally treated for diatoms analysis following Lami et al., 2000. The sample was transferred to a falcon tube and 5 ml of 30% hydrogen peroxide were added. The tubes were then heated at 50 °C for 4 h and left to settle for at least 24 h (to allow the sedimentation). The supernatant was removed and the sample was washed at least twice with distilled water. The sediment was then diluted in 10 ml of distilled water and, using a pipette, an aliquot of the sample was placed on a coverslip and left to dry at a temperature of approximately 50 °C. After the evaporation, a drop of high refractive resin (Naphrax) was placed on the coverslip that was then laid on a glass slide and let to dry overnight. Diatoms were counted and their occurrence was recorded. Finally, diatoms were identified to the lowest

possible taxonomic level using reference books and images (e.g. Krammer and Lange-Bertalot, 1986; Krammer and Lange-Bertalot, 1988; Krammer and Lange-Bertalot, 1991a, 1991b).

3.7. XRF

Sediment samples were analysed using a non-contact micro-XRF scanning spectrometer on the untouched surface of the core. Once the outline of the segment had been created on a polystyrene sample holder, the segment under examination was laid down and positioned at the most suitable point for analysis. The elemental composition of the sediment samples was analysed in air by using a CRONO X-ray spectrometer by Bruker with rhodium anode. A 0.5 mm collimator, 200 μA current power by 40 kV, and an acquisition time of 200 ms were employed for the analysis. The analysis setup was optimized to collect the main relevant elements: K, Si, Ca, Fe, Mn and Ti. Two different complete line scans were collected per sample for reproducibility, and the obtained values were averaged. Preliminary data interpretation was done using proprietary software; further elaboration was realized with ESPRIT Bruker and Origin 8.5 to enhance graph readability. The results were subsequently reported as signal ratios, referred to Ti (i.e. Si/Ti, K/Ti, Ca/Ti, Mn/Ti and Fe/Ti). Ti was selected as a normalizing element because it is considered conservative, predominantly detrital in origin, and minimally affected by post-depositional mobility (Boës et al., 2011). Moreover, normalization to Ti reduces the influence of grain-size variability and sediment dilution effects, allowing a more robust comparison of geochemical signals through the sedimentary sequence. In this context, Fe/Ti and Mn/Ti ratios may provide information on redox-sensitive processes and changes in bottom-water oxygenation, Si/Ti reflects variations between biogenic silica production and siliciclastic input, Ca/Ti is indicative of changes in carbonate precipitation and/or endogenic productivity, and K/Ti represents variations in fine-grained terrigenous input and weathering intensity within the catchment (as synthesized in Table S1).

Principal Component Analysis (PCA) was applied to explore covariance patterns among geochemical variables (element to Ti ratio in this paper) and to identify dominant geochemical associations reflecting sediment sources and depositional processes. PCA has been widely used in lacustrine sediment studies for dimensionality reduction and proxy interpretation (Grygar and Popelka, 2016; Reimann et al., 2008). The geochemical variables were standardized and log-transformed to reduce data skewness and heteroscedasticity, and to improve the robustness and interpretability of the PCA results. The dataset was transformed into z-scores prior to the analysis. The number of components was determined by retaining only those with eigenvalues greater than 1, according to the Kaiser–Gutmann criterion. The PCA was performed using packages implemented in the R statistical environment (R Core Team, 2023), following standard procedures for multivariate analysis of geochemical datasets.

4. Results

4.1. Stratigraphy

The sampled core had a total length of 105 cm. The first 45 cm were composed mainly of coarse debris like gravels and blocks with a diameter of a maximum of 15–20 cm. Underlying this thick layer, as reported in Fig. 4, there is a layer of 24 cm of non-laminated silty clays with a colour of 7.5YR 5/3 further down until the depth of 84 cm there is a layer 15 cm thick of laminated silty clays with a colour of 7.5YR 6/4. At 84 cm, an abrupt event is marked by a shift to coarser sedimentation, consisting of 4 cm of silty clays with gravel and sand, and a distinctly more reddish colour (5YR 3/3). The last 17 cm of the core are composed of sediment similar to the second layer, with silty clays with a colour of 7.5YR 3/3. The bottom of this layer of silty clay is overlies large blocks and boulders that made it impossible to continue the coring. The

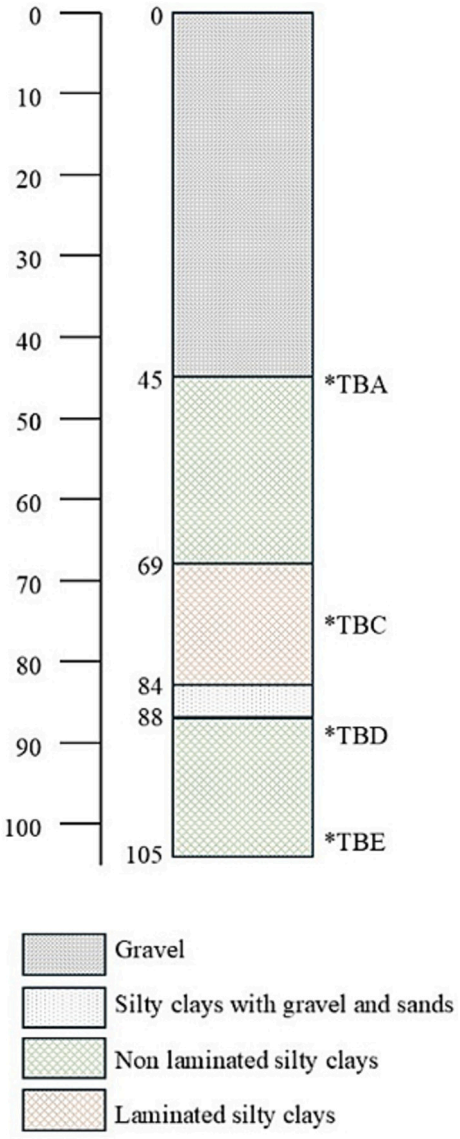

Fig. 4. Stratigraphy of the whole core obtained through the software Tilia 3.0.3.

described stratigraphy suggests, from the bottom to the surface, a lacustrine environment with almost continuous sedimentation from the base to the depth of 45 cm, except for the discontinuity between 88 and 84 cm, where the occurrence of a sudden change in sedimentation after an erosive phase is evident. A markedly different colour suggests an interruption of the sedimentation. The latter 45 cm represents the current discontinuous fluvial sedimentation.

4.2. Radiocarbon dating

The amount of terrestrial vegetal macroremains was low in all the sediments and therefore we decided to date sample of bulk sediment including all the terrestrial vegetal macroremains as reported in Table 1. Despite it is well known that bulk sediment can give much older age than the correct one for the possible contamination with “old carbon”, the obtained $\delta^{13}C$ values ranging between −23.3‰ and − 24.1‰ are comparable to standard values for vegetation (Smith and Epstein, 1970) probably because the selected samples contain a quite high number of terrestrial plants macroremains (but unfortunately not enough to date alone themselves). Moreover, the obtained ages are all in chronological sequence with the depth that give us a certain confidence in regards. In

Table 1
Depth (average), laboratory codes, conventional ages, radiocarbon calibrated ages (average), and δ13C of dated samples.

Depth (cm)	Lab code	Conventional Age (BP)	Calibrated Age (95.4% Cal BP)	δ13C
46	Beta - 561,801	8100 ± 30	9.046 ± 46	−24.1‰
79	Beta - 643,178	11,160 ± 30	13.095 ± 53	−23.3‰
90	Beta - 561,800	16,540 ± 50	19.944 ± 202	−23.8‰
104	Beta - 643,179	25,150 ± 100	29.481 ± 322	−24.0‰

addition, according the recommendations of Strunk et al. (2020) about the reliability of the bulk sediments for the radiocarbon dating, in our case the OM is high in all the dated samples. Therefore, although based on bulk analysis, the chronology reported in this work results reasonably consistent and acceptable (Taylor et al., 1987). The onset of the lacustrine sedimentation is set around 29,600 cal BP (see Table 1) during the Pleistocene well before the Last Glacial Maximum (LGM) while the end of the lacustrine story is set around 9100 cal BP, during the early Holocene. As shown in the Age-Depth curve of Fig. 3, the layer between 84 and 88 cm marks an interruption in sedimentation lasting least 4800 years. This is also evident form the sedimentation rate: in the layers above 84 cm it is about ca of 0.08 mm per year, whereas below 88 cm it is much slower (ca 0.01 mm per year).

4.3. Sediment characteristics

The laboratory analyses (Fig. 5) revealed a less well-sorted grain size distribution than that observed visually in the core, except for the 84–88 cm layer, which contains more than 10% gravel. The core below the upper coarse sediment unit shows a relatively constant content of clay (ca 20%) with a slight peak at 52 cm (ca 26%). Silt content is more variable, ranging from ca 9% in the gravel -bearing 84–88 cm layer to nearly 23% between 49 and 52 cm. Fine sand also fluctuates markedly, with the highest proportion (ca 60%) at 48 cm and the lowest (ca 42%) at 52 cm. The OM content (percentage) ranges from less than 2 at 68 cm to more than 22 at 78 cm, with 4 relative peaks (>15%) of OM content at 102–103; 50–51; 48 and 46 cm, and low values (<5%) at 80, 71 and 66 cm. The IC (carbonates) content is quite low, averaging about 5% with values ranging from ca. 1% at 95 cm to 7.3% at 45 cm. It is also notable that IC content decreases with depth from 7% in the upper part of the core to 3% at the bottom.

4.4. Chlorophill and carotenoids

In Fig. 5, total pigments, expressed as chlorophyll derivates (CD), total carotenoids (TC), and the ratio between chlorophyll derivates and total carotenoids (CD/TC) are also reported. CD shows great variability in the core ranging from non-detectable values at 51–52 cm to 127 mg g^{-1} OM at 69 cm. Other abundance peaks (>15 mg g^{-1}) are present at 73, 89, 96, 98 and 99 cm. The total carotenoids show the same pattern, although at much lower concentrations (almost one order of magnitude less), with a minimum (non-detectable values) at 51–52 cm, and a maximum at 69 cm (16 mg g^{-1} OM). Other abundance peaks (> 5 mg g^{-1}) are observed at 54, 98 and 99 cm. The CD/TC ratio (where TC are multiplied per 100) points out that TC exceeds CD only between 55 and 57 cm.

4.5. Macroremains

As shown in Fig. 6, macroremains are generally rare and their abundance decreases with depth, although in several levels they were not found. At only 5 depths, more than 10 macroremains were found: 48, 51,63, 78 and 81 cm. The presence of wood fragments was observed at

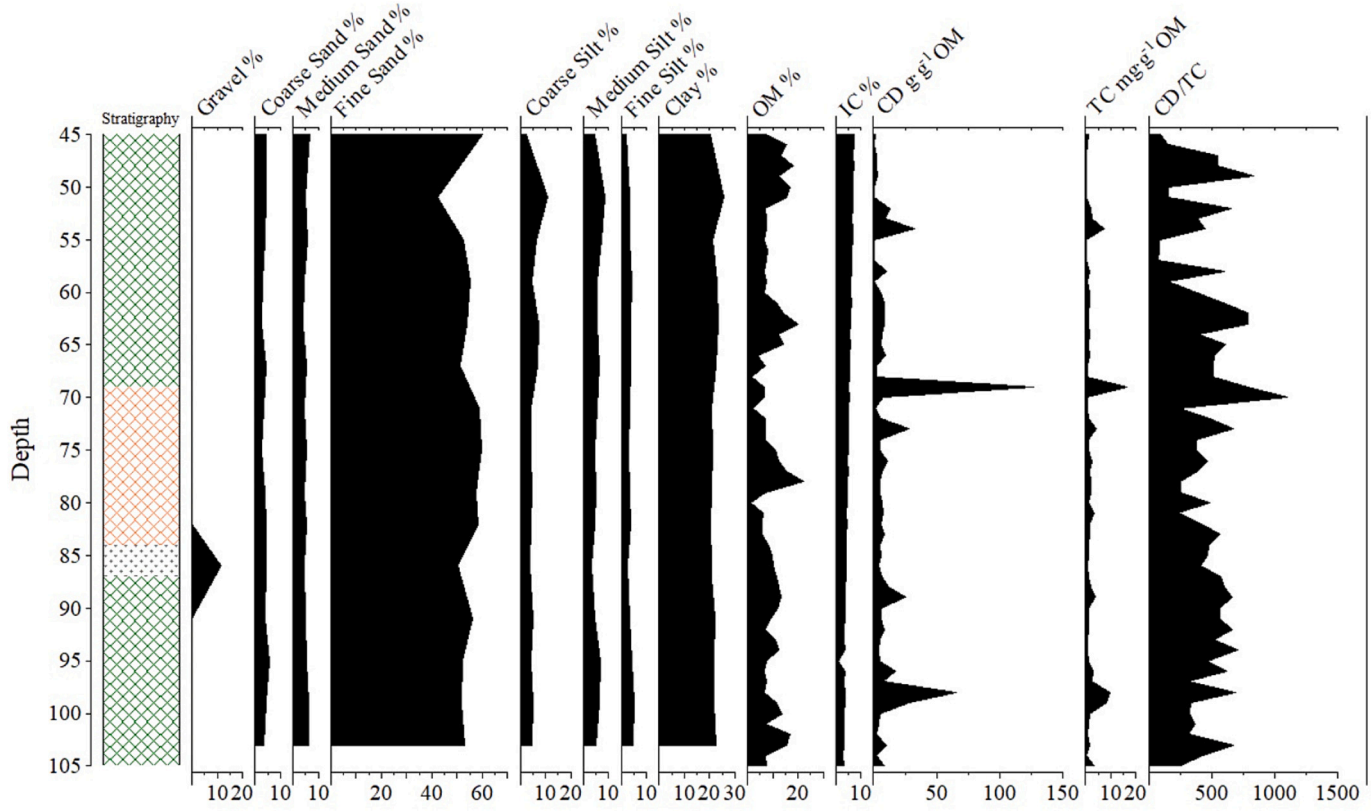

Fig. 5. Stratigraphy, grain size classes (%); OM and IC (%), clorophyll derivates (CD, gg^{-1} OM), total carotenoids (TC, mgg^{-1} OM) and the ratio CD/TC.

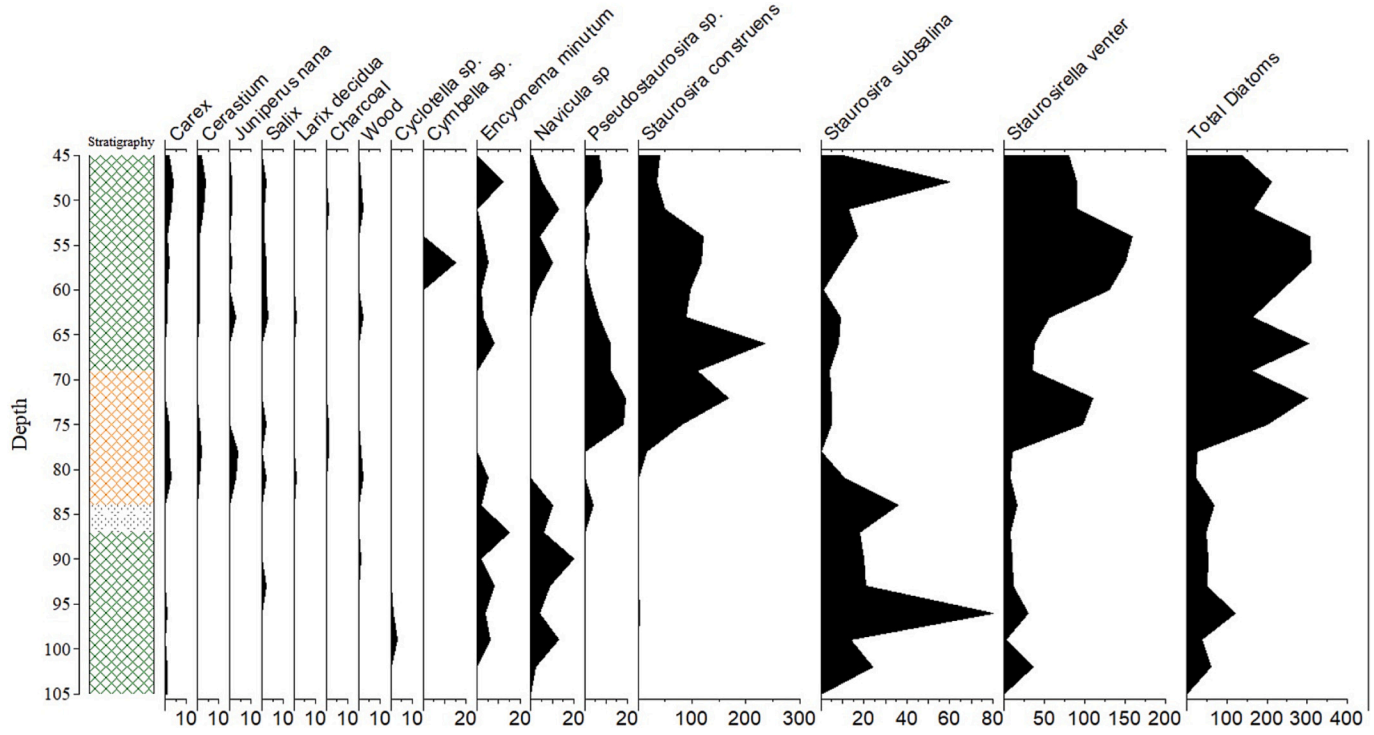

Fig. 6. Stratigraphy, macroremains and the main and total diatoms found in the core. Through the core. Macroremains and diatoms are expressed as counted numbers.

48, 51, 63, 78, 81 and 90 cm, while charcoal was present at 51, 75 and 78 cm. Particularly noteworthy is the presence *Larix decidua* at the same depth where other unidentifiable wood fragments were found, down to 81 cm. The shrub *Juniperus nana* was found until 81 cm of depth, with abundance peaks at 63 and 78–81 cm. The presence of herbaceous as *Carex* sp., *Cerastium* sp., *Salix* sp., is less surprising and more abundant in the upper part between 45 and 51 cm and 75–81 cm.

4.6. Diatoms

The total diatoms content is higher in the upper part of the core, up to 80 cm, where it suddenly decreases and then remains low to the bottom, with a relative maximum at 96 cm (Fig. 6). The diatoms are unfragmented, and it was possible to identify at least their genera of almost all cases. The most abundant taxa are *Staurositella venter* and *Staurosira subsalina* which were found at different abundance, but through the entire core.

Regarding *Staurosira subsalina,* three abundance peaks occur in the upper core (48–51 cm), at the end of the coarser episode (84–87 cm) and between 90 and 102 cm, with the highest value at 96–99 cm.

Staurositella venter is abundant in the upper part, reaching its maximum at 54–57 cm. This is followed by a period of relative paucity between 63 and 72 cm, a second peak between 72 and 78 cm and then a sharp decline.

Staurosira costruens is notably present and abundant until 81 cm, with higher peaks at 44–57, 66–69 and 72–75 cm. Downwards, only at 96–99 cm, it was found (only 2 units).

Pseudostaurosira sp. is almost continuous from the 48 to 78 cm, but it is absent below this depth,with the exception of the coarser layer between 84 and 87 cm.

Encyonema minatum, and *Navicula* sp. is present discontinuously and at roughly one order of magnitude lower abundance, with gaps between 69 and 81 cm for the former and between 63 and 84 for the latter. *Encyonema minatum* is absent also at the bottom of the core. Differently, *Cymbella* sp. has been found only between 57 and 60 cm, whereas *Cyclotella* sp. between 96 and 102 cm.

4.7. XRF

Fig. 7 shows the trends of several elemental ratios obtained through XRF analysis, including Fe/Ti, Ca/Ti, K/Ti, Si/Ti and Mn/Ti. The Fe/Ti signal ratio remains relatively stable across the sediment core, fluctuating between 25 and 35. The lowest ratio levels were observed between 88 and 92 cm, whereas a general increase was recorded between 52 and 65 cm. The Ca/Ti ratio decreases with depth, starting at about 1.5 at 45 cm and steadily declining to values close to 0.5 at 105 cm, mirroring the trend of IC. The K/Ti signal ratios showed marked decreases at about 50, 62, 69 and 89 cm. The Si/Ti ratio shows more pronounced fluctuations, ranging from 0.4 to 0.8, with significantly higher values between 52 cm and 60 cm, and between 72 and 76 cm. Although Mn/Ti varies considerably throughout the core, it shows a marked decrease is observed between 84 and 88 cm, followed by a general increase in the more recent sediment. Interestingly, Mn/Ti and Fe/Ti exhibit a significant negative correlation ($r = -0.63, p < 10^{-7}$), indicating that increases in Fe are associated with decreases in Mn.

5. Discussion

5.1. The glacial evolution of GZG: The existence of the "Nunatak Oasi" during the LGM

According to the glacial map of Ehlers et al., 2011, not shown) and the trimline position (Fig. 1c), the core site lay beneath the ice during the LGM, whereas an extensive nunatak around the Gran Zebrù peak remained ice-free. Evidence of a possible major glacier retreat, or even complete deglaciation, in the upper Val Cedec has been hypothesized by Forte et al. (2021) to explain a large debris body beneath the current eastern sector of the Gran Zebrù Glacier (GZG in Fig. 1c), although its age remains still unknown. Deglaciation chronologies for the high elevation inner Valtellina are scarce. The GZG and the other glaciers of the Cedec valley were connected along the valley floor and flowed into the Forni glacier around 15,000 cal BP, but by 13,700 cal BP the Cedec Glacier had separated from the Forni Glacier and terminated somewhere

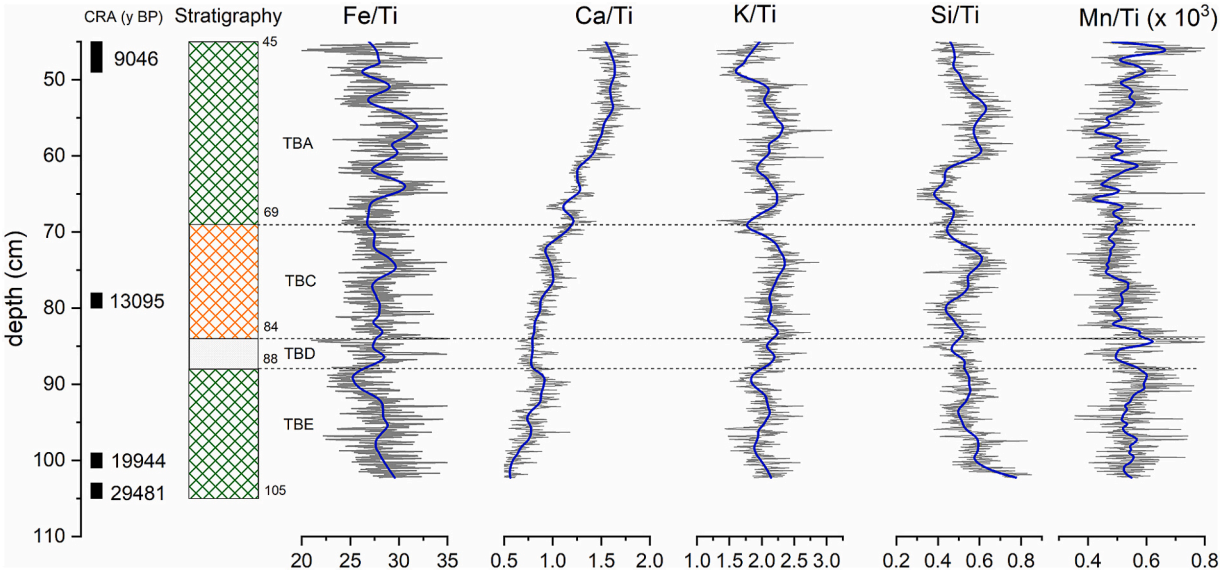

Fig. 7. Stratigraphy geochemical ratios trend (Fe/Ti; Ca/Ti, K/Ti;i/Ti, Mn/Ti), expressed as adimensional numbers.

along the Cedec valley floor (Fig. 1b). The only massive glacier retreat in the area occurred later, between 9500 and 4100 cal BP, when the nearby Forni Glacier underwent its largest Holocene recession, documented by buried *Pinus cembra* wood dated 4100 cal BP at almost 2400 m a.s.l. (Pelfini et al., 2014).

Despite of these constrains, the basal age of the fine sediments in our core, derived from the age-depth model of Fig. 3, indicates that the site was already ice-free by 30,000 cal BP. The non-laminated fine sediments between 105 and 88 cm depth resemble the grain size distribution of a modern lake near our site, where fine sand dominated over clay. As also testified by the other proxies found in the sediments, we hypothesize the presence of a small paleolake. There is no evidence of glacier burial until 18,500 cal BP, when these fine sediments were overlain by the coarser layer between 88 and 84 cm. At that time, the Cedec and Forni Glaciers were joined at the valley floor, yet the site under study apparently remained ice-free. The poorly sorted coarse deposit between 88 and 84 cm is most plausibly the product of a mass movement (debris flow) or fluvial event that infilled the depression hosting the paleolake. A current drop in Mn supports this interpretation: high-energy events can transport coarse material, while depleting mobile elements such as Mn, which are usually associated with finer fractions or occurred in solution. The reddish colour of this layer suggests an intense weathering that, considering the closer ^{14}C ages, lasted at least 4800 years long. The negligible change in iron content detected by XRF in this layer is best explained by structural modifications of iron-bearing minerals rather than by a change in overall Fe abundance. This hiatus probably spans 18,500–13,700 cal BP, a period without recorded glacial advances in the area (Longhi and Guglielmin, 2021). Subsequently, between 84 and 69 cm, laminated fine sediments were deposited at higher rate than in the deeper unit, reflecting very low energy conditions. The top of this laminated unit dates to ca. 11,900 cal BP, only a few centuries younger than the more widespread glacial advance in the area, corresponding to the Younger Dryas period. (i.e.Longhi et al., 2020). Overlying sediments are not laminated, but show greater grain size variability. Lacustrine deposition ceased at ca 9000 cal BP, shortly after (few centuries) the most extensive Holocene glacial event (Longhi et al., 2020). Above the lacustrine sequence lies 45 cm-thick unit of coarse debris, indicative of a high-energy depositional regime, likely driven by mass wasting or fluvial activity, reflecting a recent and rapidly changing environment. Although the contact between units is difficult to pinpoint, its irregular, sharp nature suggests an erosional surface. Unfortunately, the absence of ^{14}C ages in the upper unit prevents precise dating of this event. Whether during the Little Ice Age (LIA), when GZG merged with Cedec glacier (CdG) and reached ca 2680 m asl with its front, the paleolake was still present or buried by the glacier, remains unknown. Historical documents indicate that the area was likely ice-covered by the GZG until 1931 (Fig. 1c) and lay close to the glacier front through the 1950s and even the early 1960s. During this period of rapid glacial retreat, the eastern part of the GZG was entirely buried by sediments, making it likely that the coarse upper unit was deposited during this phase.

5.2. Paleoenvironmental conditions between 30,000 and 9000 cal BP

Through the different biotic and abiotic proxies analysed, we tentatively reconstruct the different environmental conditions of the lake. The continuous presence of *Staurosirella venter,* a strictly aquatic species, indicates that the basin never fell completely dry once lacustrine conditions were established. Other dominant diatoms can give more details about the level of the water and of the edaphic conditions of the paleolake. Our findings show that the core is dominated by fresh-brackish water diatoms, particularly from the *Staurosira* genus. Most of the taxa found in our samples are cosmopolitan, commonly present in lake environments across middle to high latitudes in the Northern Hemisphere, as documented by several studies (Blake Jr et al., 1992; Cremer et al., 2001; Cremer and Wagner, 2004; Kienel and Kumke, 2002; Lotter and Biegler, 2000; Medvedeva et al., 2009; Smol et al., 2005; Solovieva et al., 2008; Van Dam et al., 1994).

In terms of water level, the presence of *Staurosira subsalina* is particularly noteworthy. This species, typically associated with shallow, slightly saline environments, suggests that the lake was especially shallow and enriched in salts, possibly as a result of higher temperatures. Conversely, the prevalence of *Staurosira construens*, a species typically associated with shallow, clear waters and lower salinity, points to less warm climatic periods. Our data showed that from the base of the core up to 81 cm (ca 30,000–13,700 cal BP) the assemblage is dominated by *Staurosira subsalina. Staurosira construens* is absent and *Staurosirella venter* greatly reduced, implying a long phase of extremely shallow, warm water.

A more recent phase, between 48 and 51 cm depth, corresponding to approximately 9300 to 9600 cal yr BP, is characterized by the dominance of *Staurosira subsalina*, alongside the presence of both *Staurosirella venter* and *Staurosira construens*. This assemblage could suggest that the lake was less shallow and cooler compared to earlier phases.

Our macroremain-based reconstruction of the surrounding

environment aligns with the observations of Carcaillet and Blarquez (2017), who documented the presence of trees and shrubs around nunataks, even above glacial surfaces, in the western French Alps, although at a lower elevation (approximately 2200 m a.s.l.).

At Gran Zebrù nunatak, near 700 m higher in elevation, the macroremains identified suggested the existence of some trees mixed with a thermophilous shrub, as *Juniperus nana,* mainly in the upper core above the 84 cm. In particular, they are more abundant between 84 and 78 cm, 66 and 63 cm and subordinately between 54 and 51 cm, that corresponds respectively to 13,700-13,000, 11,500-11,000- and 10,000–9600 cal BP, respectively. It is also worth noting that that an unidentified wood fragment was found at 90 cm, corresponding to 19,900–19,600 cal BP, in the middle of the Last Glacial Maximum. In addition, the presence of charcoal between 81 and 75 cm, corresponding to 13,500 and 12,600 cal BP, indicates the occurrence of natural fires in this harsh periglacial environment.

The absence of macroremains between 84 cm and 88 cm aligns with the abrupt shift in sedimentation observed in this interval, possibly reflecting a period of increased water energy. The presence in the core further suggests that fire events, whether natural or anthropogenic, may have played a role in shaping the vegetation and sedimentation dynamics, as seen in other alpine lake records (Finsinger et al., 2006).

5.3. Chemical inferences on paleoclimatic evolution of the Gran Zebrù Nunatak

Additional insights into past environmental and climatic dynamics are provided by the geochemical composition of the sediment core. A strong positive correlation ($r = 0.892$) between carbonates (determined via LOI) and the Ca/Ti ratio (determined via XRF) indicates a significant input of calcium carbonate into the lake. Both Ca/Ti and carbonate content show a progressive increase from the bottom to the top of the core. An increase in the Ca/Ti ratio in alpine lacustrine or fluvial sediments may be consistent with warmer climatic conditions, although it should not be interpreted as a direct or exclusive proxy for temperature (Grygar and Popelka, 2016). Higher Ca/Ti values could reflect enhanced carbonate production or precipitation, potentially linked to increased biological activity or evaporation during warmer periods (Bliedtner et al., 2021; Haberzettl et al., 2007;). The carbonate accumulation in the sediment record may result from both detrital input from carbonate bedrock in the catchment and authigenic precipitation within the lake. The presence of limestone units in the surrounding area suggests that a detrital contribution to Ca cannot be excluded. However, several lines of evidence support a predominantly authigenic control on Ca/Ti variability: (i) Ca/Ti is not correlated with terrigenous indicators such as K/Ti and Fe/Ti; (ii) Ca/Ti co-varies with inorganic carbon content, indicating in situ carbonate accumulation. The Ca/Ti signal is primarily expressed in PC2 (Fig. S1), which is independent from the main terrigenous component (PC1) and shows correspondence with hemispheric/global paleotemperature records. These observations suggest that carbonate precipitation was mainly driven by lake-internal processes, likely modulated by temperature-dependent productivity and/or carbonate saturation, although episodic detrital inputs from carbonate lithologies cannot be fully excluded. In our case, the decoupling observed between IC and biological proxies in Fig. 5 may suggest that the higher Ca/Ti values may be associated with enhanced carbonate precipitation, not directly coupled with organic productivity indicators such as organic matter content or pigment concentrations but probably primarily controlled by physico-chemical conditions (e.g., temperature, alkalinity and carbonate saturation, see Bliedtner et al., 2021; Haberzettl et al., 2007), which may be indirectly influenced by biological activity but do not require a synchronous increase in organic matter accumulation.

The Si/Ti ratio presents a more complex pattern. The lack of correlation with total diatom abundance suggests that the silica input may be only partially biogenic, and likely includes a significant allochthonous siliciclastic component. Still, this record should be interpreted with caution. Previous studies (Flower, 1993; Ma et al., 2023) have shown that the preservation of diatom frustules strongly depends on the chemical conditions of the lake water, as frustules may partially dissolve post-deposition, complicating its paleoenvironmental interpretation.

Interestingly, Fe and Mn display a clear negative correlation throughout the core ($r = -0.634$). Being redox-sensitive elements, this pattern indicates that their distributions are influenced by fluctuations in redox conditions within the lake. Elevated Fe concentrations (accompanied by lower Mn) suggest less oxygenated waters, consistent with a shallow, thermally stratified lake under warmer conditions (Naher et al., 2013). However, such changes may also reflect seasonal variability, as Fe and Mn are especially responsive to summer redox dynamics. In the GZN record, Fe and Mn show marked variability throughout the core, likely capturing short-term summer climatic fluctuations superimposed on a broader warming trend, as indicated by the increasing Ca/Ti ratio.

Principal component analysis of the elemental ratios shows that the first two components (PC1 (49%) and PC2 (21%) together explain roughly 70% of the total variance (see Table S2). PC1 is dominated by strong positive loadings of Fe/Ti (0.914) and K/Ti (0.855) and a strong negative loading of Mn/Ti (−0.793), consistent with the Fe—Mn negative correlation previously observed (see Table S3). Core fluctuations in PC1 (Fig. S2) may be interpreted as changes in lake-water oxygenation: higher PC1 scores indicate more reducing (less oxygenated) conditions, most evident at 54–61 cm and 71–76 cm, with local minima at 60–63 cm, 68–71 cm, and 87–91 cm. Therefore, PC1 may capture short-term, site-specific hydroclimatic variability.

PC2, which accounts for 21% of the variance, is characterized by a strong positive loading for Ca/Ti (0.921) and a moderate negative loading for Si/Ti (−0.364). The PC2 profile (Fig. 8) closely mirrors the temperature reconstructions of Davtian and Bard (2023) based on Greenland ice cores (GISP2 (9000–10,000 cal BP) and NGRIP (10,000–30,000 cal BP)) and aligns well with the records of Kindler et al. (2014) and Kobashi et al. (2017). Higher PC2 values coincide with warmer intervals, a correspondence that is evident at least since ~26,700 cal BP and further supported by parallel changes in diatom assemblages and woody macro-remain abundance.

Although the age-depth model assumes linear sedimentation in two core segments and thus carries some uncertainty, the strong agreement between PC2 and hemispheric/global temperature records enforces the chronology. We infer that PC2 records a broader regional climate signal, superimposed on the finer-scale, localized fluctuations captured by PC1.

5.4. Why a nunatak can provide more favourable climatic conditions?

The paleoclimatic signal from the site investigated in this paper can be explained by the nunatak unique micro climate: the rock is sheltered from wind and, more crucially, receives solar incoming radiation that is repeatedly reflected by the surrounding ice. On Antarctic nunataks, the surface ground temperature can be up to 25 °C higher than air temperature, and normally 15 °C higher in summer, creating hotspots of microbial diversity (Harris and Tibbles, 1997). In addition to the nunatak effect itself, we must also consider that south-facing slope receives greater solar radiation, which can raise soil temperature by more than 8 °C for several hours per day in summer season, with a mean summer surface temperature 2–4 °C higher than air (Scherrer and Körner, 2010). Therefore, if we account for the nunatak effect, we can reasonably expect the ground-surface temperature in summer to be at least 10 °C higher than the air temperature.

6. Conclusion

In this paper, we provided evidence, through a multiproxy approach, that a “cryptic refugium” or better a “nunatak refugium” according to Holderegger and Thiel-Egenter (2008) with warm ground surface and freshwater lake in the inner central European alps existed during the

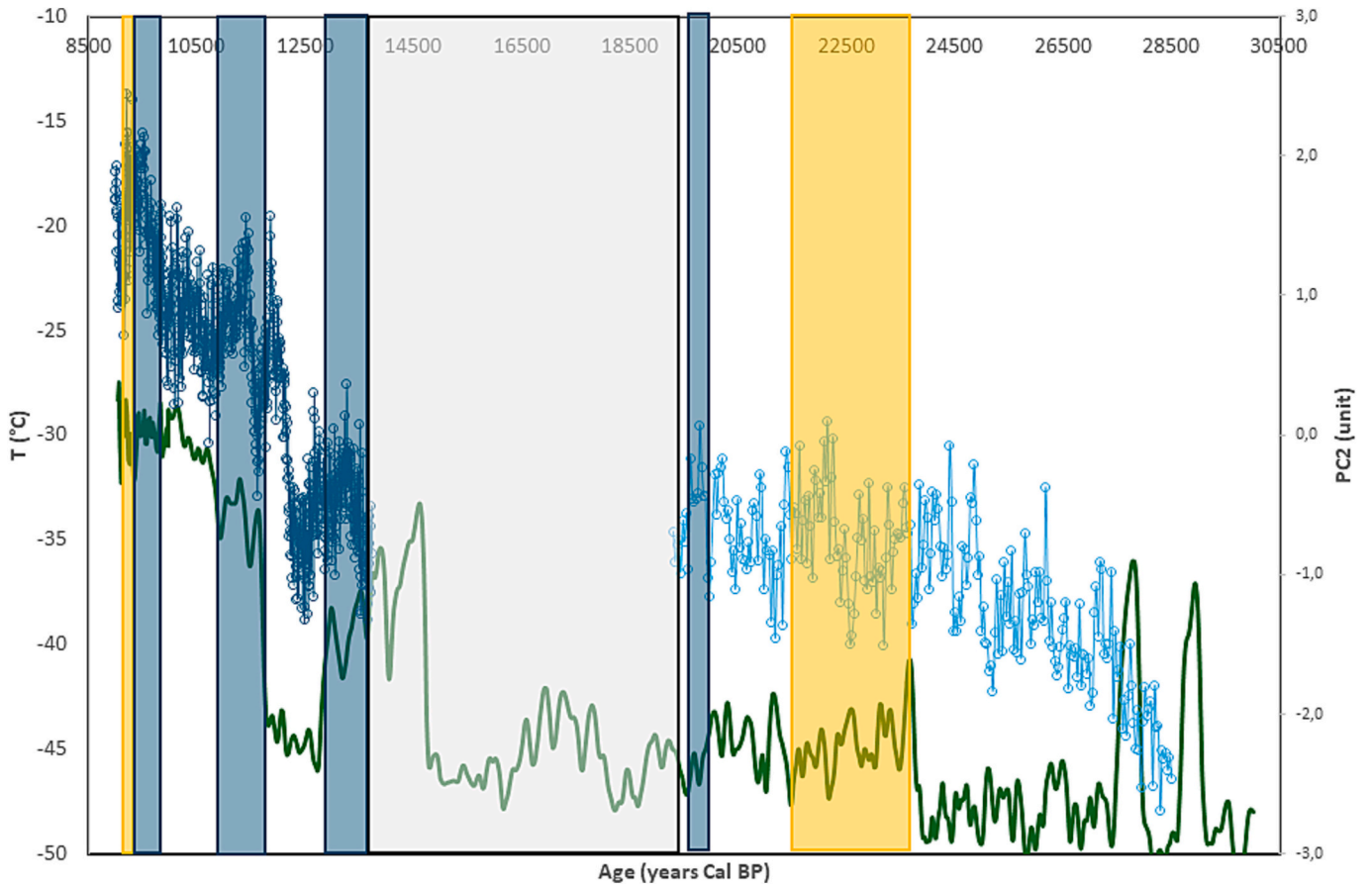

Fig. 8. Paleotemperature reconstruction according to Davtian and Bard (2023) based on Greenland ice core isotopes (green line) and PC2 of chemical composition of our core according the depth-age linear regressions of Fig. 3 (blue for the upper 84 cm and light blue between 89 and the bottom). Orange bars indicate warmer and dry periods in which *Staurosira subsalina* is dominant while blue bars indicate periods in which the forest was surrounding to our lake. Grey bar indicates the hiatus of sedimentation in which a quite strong weathering of the debris flows material suffered probably in the warmer period around 14,600 and 13,900 cal BP. (For interpretation of the references to colour in this figure legend, the reader is referred to the web version of this article.)

Last Glacial Maximum, also favored by the effect of the surrounding ice and the south-facing slope.

Plant macroremains indicate the presence of trees and shrub species, such as *Larix decidua* and *Juniperus nana*, suggesting that warmer periods allowed the persistence of this cryptic refugium at high altitude, particularly between 13,700-13,000, 11,500–11,000 and 10,000–9600 cal BP. During these periods, glaciers flowed along the valley floor and surrounded the nunatak. Weathering of the deposits dated between 18,500 and 13,700 cal BP suggests the continued existence of the refugium at GZN. Even earlier, from 30,000 cal BP to 13,700 cal BP, the dominance of *Staurosira subsalina* indicates the presence of a very shallow and relatively warm lake. Furthermore, the recovery of an unidentified wood fragment during the middle of the Last Glacial Maximum (19,900–19,600 cal BP), supports the persistence of cryptic-refugium conditions.

The use of XRF analyses with the other biological proxies allowed the reconstruction of the local paleoclimate of the area through the PC2 profile (Fig. 8) that closely mirrors the regional temperature reconstructions of Davtian and Bard (2023). Periods characterized by higher PC2 values coincide with warmer intervals, at least since ~26,700 cal BP, and are further supported by parallel changes in diatom assemblages and the abundance of woody macroremains.

CRediT authorship contribution statement

Mauro Guglielmin: Writing – review & editing, Writing – original draft, Visualization, Validation, Supervision, Project administration, Methodology, Investigation, Funding acquisition, Formal analysis, Data curation, Conceptualization. **Alessandro Longhi:** Writing – original draft, Visualization, Methodology, Investigation, Formal analysis, Data curation. **Eleonora Balliana:** Writing – original draft, Methodology, Formal analysis, Data curation. **Roberta Bettinetti:** Writing – review & editing, Writing – original draft, Methodology, Data curation. **Carlotta Santolini:** Writing – original draft, Methodology, Formal analysis, Data curation. **Dario Battistel:** Writing – review & editing, Writing – original draft, Visualization, Validation, Supervision, Resources, Project administration, Methodology, Formal analysis, Data curation, Conceptualization.

Declaration of competing interest

The authors declare that they have no known competing financial interests or personal relationships that could have appeared to influence the work reported in this paper.

Acknowledgments

We want to thank the Stelvio National Park (PNS) for the logistical support during this research in particular during the project “Glacier CC” funded by Ersaf-Parco nazionale dello Stelvio.

We want to thank the Editor and the two anonymous reviewers for their precious suggestions, comments and corrections that improved significantly the manuscript.

Appendix A. Supplementary data

Supplementary data to this article can be found online at https://doi.org/10.1016/j.catena.2026.110032.

Data availability

PC2values (Original data) (Zenodo)

References

Adams, M.S., Guilizzoni, P., Adams, S., 1978. Sedimentary pigments and recent primary productivity in northern Italian lakes. Mem. Ist. Ital. Idrobiol. 36, 267–285.

Aitken, M.J., 1990. Science-Based Dating in Archaeology. Longman, London and New York.

Alley, R.B., Andrews, J.T., Brigham-Grette, J., Clarke, G.K.C., Cuffey, K.M., Fitzpatrick, J. J., Funder, S., Marshall, S.J., Miller, G.H., Mitrovica, J.X., Muhs, D.R., Otto-Bliesner, B.L., Polyak, L., White, J.W.C., 2010. History of the Greenland ice sheet: paleoclimatic insights. Quat. Sci. Rev. 29 (15–16), 1728–1756. https://doi.org/10.1016/j.quascirev.2010.02.007.

ASTM 2007. Standard Test Method for Particle Size Analysis of Soil. ASTM D422–63.

Ballantyne, C.K., 1998. Age and significance of mountain-top detritus. Permafr. Periglac. Process. 9, 327–345. Doi;10.1002/(SICI)1099-1530(199810/12)9: 43.0.CO;2-9.

Battarbee, R.W., Juggins, S., Gasse, F., Anderson, N.J., Bennion, H., Cameron, N.G., Ryves, D.B., Pailles, C., Chalié, F., Telford, R., 2001. European Diatom Database (EDDI). An information System for Palaeoenvironmental Reconstruction.

Birks, H.H., 1994. Plant macrofossils and the nunatak theory or per-glacial survival. Dissertationes Botanicae 234, 129–143.

Birks, H.J.B., Willis, K.J., 2008. Alpines, trees, and refugia in Europe. Plant Ecol. Diversity 1 (2), 147–160.

Biskaborn, B.K., Herzschuh, U., Bolshiyanov, D., Savelieva, L., Diekmann, B., 2012. Environmental variability in northeastern Siberia during the last ~13,300 yr inferred from lake diatoms and sediment–geochemical parameters. Palaeogeogr. Palaeoclimatol. Palaeoecol. 329–330, 22–36.

Blaauw, M., 2010. Methods and code for 'classical' age-modelling of radiocarbon sequences. Quat. Geochronol. 5 (5), 512–518. https://doi.org/10.1016/j.quageo.2010.01.002.

Blaauw, M., Christen, J.A., Mauquoy, D., van der Plicht, J., Bennett, K.D., 2007. Testing the timing of radiocarbon-dated events between proxy archives. The Holocene 17, 283–288.

Blake Jr., W., Boucherle, M.M., Fredskild, B., Anssens, A.A., Smol, J.P., 1992. The geomorphological setting, glacial history and Holocene development of Kap Ingleneld se Inglefield land, North-West Greenland. Medd. Groenl. Geosci. 27, 1–42.

Bliedtner, M., Struck, J., Strobel, P., Salazar, G., Szidat, S., Bazarradnaa, E., Lloren, R., Dubois, N., Zech, R., 2021. Late Holocene climate changes in the Altai region based on a first high-resolution biomarker isotope record from Lake Khar Nuur. Geophys. Res. Lett. 48, e2021GL094299.

Blytt, A., 1882. Die Theorie der wechselnden kontinentalen und insularen Klimate. Botanische Jahrbücher 2, 1–50.

Boës, X., Rydberg, J., Martinez-Cortizas, A., Bindler, R., Renberg, I., 2011. Evaluation of conservative lithogenic elements (Ti, Zr, Al, and Rb) to study anthropogenic element enrichments in lake sediments. J. Paleolimnol. 46 (1), 75–87. https://doi.org/10.1007/s10933-011-9515-z.

Brochmann, C., Gabrielson, T.M., Nordal, I., Landvik, J.Y., Elven, R., 2003. Glacial survival or *tabula rosa*? The history of North Atlantic biota revisited. Taxon 52, 417–450.

Carcaillet, C., Blarquez, O., 2017. Fire ecology of a tree glacial refugium on a nunatak with a view on Alpine glaciers. New Phytol. 216, 1281–1290.

Carcaillet, C., Latil J.L. Abou, S., Adam, A., Ghaleb, B., Magnin, F., Roiron, P., Aubert, S., 2018. Keep your feet warm? A cryptic refugium of trees linked to a geothermal spring in an ocean of glaciers. Glob. Chang. Biol. 24, 2476–2487.

Cartier, R., Brisset, E., Guiter, F., Sylvestre, F., Tachikawa, E.J., Paillès, C., Bruneton, H., Bard, E., Miramont, C., 2018. Multiproxy analyses of Lake Allos reveal synchronicity and divergence in geosystem dynamics during the Lateglacial/Holocene in the Alps. Quat. Sci. Rev. 186, 60–77.

Cremer, H., Wagner, B., 2004. Planktonic diatom communities in high Arctic lakes (store Koldewey, Northeast Greenland). Can. J. Bot. 82, 1744–1757.

Cremer, H., Wagner, B., Melles, M., Hubberten, G.W., 2001. The postglacial environmental development of Raffles Sø, East Greenland: inferences from a 10,000 year diatom record. J. Paleolimnol. 26, 67–87.

Davtian, N., Bard, E., 2023. A new view on abrupt climate changes and the bipolar seesaw based on paleotemperatures from Iberian margin sediments. PNAS 120 (12), e2209558120.

Deichmann, N., Ferliga, C., Ceriani, M., Berra, F., Cariboni, M., Mazzoccola, D., Mair, V., Jadoul, F., Guerra, S., Gregnanin, A., Guglielmin, M., Longhin, M., Montrasio, A., Sciesa, E., Zappone, A., 2012. Note Illustrative della Carta geologica d'Italia alla scala 1:50.000, F. 024 Bormio. Servizio Geologico d'Italia - ISPRA. https://doi.org/10.15161/oar.it/211469.

Ehlers, J., Gibbard, P.L., Hughes, P.D., 2011. Quaternary glaciations - extent and chronology: A closer look, V. 15. Elsevier.

Finsinger, W., Tinner, W., Colombaroli, D., Vescovi, E., 2006. Fire history and vegetation response to climatic and land-use changes in southern Switzerland. Palaeogeogr. Palaeoclimatol. Palaeoecol. 237 (2–4), 253–265.

Flower, R.J., 1993. Diatom preservation: experiments and observations on dissolution and breakage in modern and fossil material. Hydrobiologia 269 (270), 473–484.

Forte, E., Santin, I., Ponti, S., Colucci, R.R., Gutgesell, P., Guglielmin, M., 2021. New insights in glaciers characterization by differential diagnosis integrating GPR and remote sensing techniques: A case study for the eastern gran Zebrù glacier (Central Alps). Remote Sens. Environ. 267, 112715.

Gjærevoll, O., 1963. Survival of plants on nunataks in Norway during the Pleistocene glaciation. In: Löve, Á., Löve, D. (Eds.), North Atlantic Biota and Their History. Pergamon Press, Oxford, pp. 261–283.

Goodfellow, B., 2007. Relict non-glacial surfaces in formerly glaciated landscapes. Earth-Sci. Rev. 80, 47–73. https://doi.org/10.1016/j.earscirev.2006.08.002.

Grygar, M.T., Popelka, J., 2016. Revisiting geochemical methods of distinguishing natural concentrations and pollution by risk elements in fluvial sediments. J. Geochem. Explor. 170, 39–57.

Guilizzoni, P., Lami, A., Marchetto, A., 1992. Plant pigment ratios from lakes sediments as indicators of recent acidification in alpine lakes. Limnol. Oceanogr. 37 (7), 1565–1569.

Haberzettl, T., Corbella, H., Frey, M., Janssen, S., Lücke, A., Mayr, C., Ohlendorf, C., Schäbitz, F., Schleser, G.H., Wille, M., Wulf, S., Zolitschka, B., 2007. Lateglacial and Holocene wet-dry cycles in southern Patagonia: chronology, sedimentology and geochemistry of a lacustrine record from Laguna Potrok Aike, Argentina. Holocene 17, 297–310. https://doi.org/10.1177/0959683607076437.

Harris, J.M., Tibbles, B.J., 1997. Factors affecting bacterial productivity in soils on isolated inland Nunataks in continental Antarctica. Microb. Ecol. 33 (2), 106–123.

Heiri, O., Lotter, A.F., Lemcke, G., 2001. Loss on ignition as a method for estimating organic and carbonate content in sediments: reproducibility and comparability of results. J. Paleolimnol. 25, 101–110.

Holderegger, R., Thiel-Egenter, C., 2008. A discussion of different types of glacial refugia used in mountain biogeography and phylogeography. J. Biogeogr. 36, 476–480. https://doi.org/10.1111/j.1365-2699.2008.02027.x.

Jackson, S.T., Lyford, M.E., 1999. Pollen dispersal models in quaternary plant ecology: assumptions, parameters, and prescriptions. Bot. Rev. 65, 39–75.

Jiménez, L., Romero-Viana, L., Conde-Porcuna, J.M., Pérez-Martinéz, C., 2015. Sedimentary photosynthetic pigments as indicators of climate and watershed perturbations in an alpine lake in southern Spain. Limnetica 34 (2), 439–454.

Jones, G.E.M., 1991. Numerical analysis in archaeobotany. In: van Zeist, W., et al. (Eds.), Progress in Old World Palaeoethnobotany. Balkema, Rotterdam.

Keith, M.L., Weber, J.N., 1964. Carbon and oxygen isotopic composition of selected limestones and fossils. Geochim. Cosmochim. Acta 28 (10–11), 1787–1816.

Kelly, M.A., Buoncristiani, J.-F., Schlüchter, C., 2004. A reconstruction of the last glacial maximum (LGM) ice-surface geometry in the western Swiss Alps and contiguous Alpine regions in Italy and France. Eclogae Geol. Helv. 97, 57–75.

Kienel, U., Kumke, T., 2002. Combining ordination techniques and geostatistics to determine the patterns of diatom distributions at Lake Lama, Central Siberia. J. Paleolimnol. 28, 181–194.

Kindler, P., Guillevic, M., Baumgartner, M., Schwander, J., Landais, A., Leuenberger, M., 2014. Temperature reconstruction from 10 to 120 kyr b2k from the NGRIP ice core. Clim. Past 10, 887–902. https://doi.org/10.5194/cp-10-887-2014.

Kobashi, T., Menviel, L., Jeltsch Thömmes, A., Vinther, B.M., Box, J.E., Muscheler, R., Nakaegawa, T., Pfister, P.L., Döring, M., Leuenberger, M., Wanner, H., Ohmura, A., 2017. Volcanic influence on centennial to millennial Holocene Greenland temperature change. Sci. Rep. 7, 1441.

Krammer, K., Lange-Bertalot, H., 1986. Bacillarophyceae 2/1. Naviculaceae. In: Ettl, H., Gerloff, J., Heynig, H., Mollenhauser (Eds.), Süsswasserflora von Mitteleuropa. Gustav Fischer Verlag, Stuttgart.

Krammer, K., Lange-Bertalot, H., 1988. Bacillarophyceae 2/2. Basillariaceae, Epithemiaceae, Surirellaceae. In: Ettl, H., Gerloff, J., Heynig, H., Mollenhauser (Eds.), Süsswasserflora von Mitteleuropa. Gustav Fischer Verlag, Stuttgart.

Krammer, K., Lange-Bertalot, H., 1991a. Bacillarophyceae 2/3. Centrales, Fragilariaceae, Eunotiaceae. In: Ettl, H., Gerloff, J., Heynig, H., Mollenhauser (Eds.), Süsswasserflora von Mitteleuropa. Gustav Fischer Verlag, Stuttgart.

Krammer, K., Lange-Bertalot, H., 1991b. Achnanthaceae, Kritische Erganzungen zu Navicula (Lineolatae) und Gomphonema. In: Ettl, H., Gerloff, J., Heynig, H., Mollenhauser (Eds.), Süsswasserflora von Mitteleuropa. Gustav Fischer Verlag, Stuttgart.

Kullman, L., 2008. Early postglacial appearence of tree species in northern Scandinavia: review and perspective. Quat. Sci. Rev. 27 (27–28), 2467–2472. https://doi.org/10.1016/j.quascirev.2008.09.004.

Lami, A., Niessen, F., Guilizzoni, P., Masaferro, J., Belis, C.A., 1994. Palaeolimnological studies of the eutrophication of volcanic Lake Albano (Central Italy). J. Paleolimnol. 10 (3), 181–197.

Lami, A., Guilizzoni, P., Marchetto, A., 2000. High resolution analysis of fossil pigments, carbon, nitrogen and Sulphur in the sediment of eight European Alpine lakes: the MOLAR project. J. Limnol. 59 (1s), 15–28.

Longhi, A., Guglielmin, M., 2021. The glacial history since the last glacial maximum in the Forni Valley (Italian Central Alps). Reconstruction based on Schmidt's hammer R-values and crystallinity ratio indices of soils. Geomorphology 387, 107765.

Longhi, A., Monticelli, D., Guglielmin, M., 2020. The use of iron chemical analysis of podzols to date the late Pleistocene-Holocene deglaciation history of the central Italian Alps. J. Quat. Sci. 35 (8), 1021–1035.

Lotter, A.F., Biegler, C., 2000. Do diatoms in the Swiss Alps reflect the length of ice-cover? Aquat. Sci. 62, 125–141.

Ma, Y., Yang, B., Zhou, N., Huang, J., Liu, S.M., Zhu, D., Liang, W., 2023. Distribution and dissolution kinetics of biogenic silica in sediments of the northern South China Sea. Front. Mar. Sci. 10, 1083233.
McCarroll, D., Ballantyne, C.K., Nesje, A., Dahl, S.O., 1995. Nunataks of the last ice sheet in Northwest Scotland. Boreas 24, 305–323. Doi;10.1111/j.1502-3885.1995.tb00782.X.
Medvedeva, L.A., Nikulina, T.V., Genkal, S.I., 2009. Centric diatoms (Coscinodiscophyceae) of fresh and brackish water bodies of the southern part of the Russian Far East. Oceanol. Hydrobiol. Stud. 38, 139–164.
Meeks, J., Moeck, C., Brunner, P., Hunkeler, D., 2017. Infiltration under snow cover: modeling approaches and predictive uncertainty. J. Hydrol. 546, 16–27.
Naher, S., Gilli, A., North, R.P., Hamann, Y., Schubert, C.J., 2013. Tracing bottom water oxygenation with sedimentary Mn/Fe ratios in Lake Zurich, Switzerland. Chem. Geol. 352, 125–133. https://doi.org/10.1016/j.chemgeo.2013.06.006.
Nelson, D.W., Sommers, L.E., 1996. Total carbon, organic carbon, and organic matter. Methods of soil analysis, part 2. In: Page, A.L., et al. (Eds.), Agronomy, 2nd ed. 9. Am. Soc. of Agron., Inc., Madison, WI, pp. 961–1010.
Öberg, L., Kullman, L., 2011. Ancient subalpine clonal spruces (Picea abies): sources of postglacial vegetation history in the Swedish Scandes. Arctic 64, 183–196.
Parducci, L., Jørgensen, T., Tollefsrud, M.M., Elverland, E., Alm, T., Fontana, S.L., Bennett, K.D., Haile, J., Matetovici, I., Suyama, Y., Edwards, M.E., Andersen, K., Rasmussen, M., Boessenkool, S., Coissac, E., Brochmann, C., Taberlet, P., Houmark-Nielsen, M., Larsen, N.K., Orlando, L., Gilbert, M.T., Kjær, K.H., Alsos, I.G., Willerslev, E., 2012. Glacial survival of boreal trees in northern Scandinavia. Science 335 (6072), 1083–1086. https://doi.org/10.1126/science.1216043. Mar 2.
Paus, A., 2010. Vegetation and environment of the Rødalen alpine area, Central Norway, with emphasis on the early Holocene. Veg. Hist. Archaeobotany 19, 29e51.
Paus, A., Velle, G., Berge, J., 2011. The lateglacial and early Holocene vegetation and environment in the dovre mountains, Central Norway, as signalled in two Lateglacial nunatak lakes. Quat. Sci. Rev. 30, 1780e1796.
Pearsall, D.H., 2000. Paleoethnobotany: A Handbook of Procedures, 2nd edition. Academic Pres, San Diego.
Pelfini, M., 1992. Le fluttuazioni glaciali oloceniche nel Gruppo Ortles-Cevedale (settore lombardo). Università degli Studi di Milano. Earth Science Department. PhD thesis IV cycle.
Pelfini, M., Leonelli, G., Trombino, L., Zerboni, A., Bollati, I.M., Merlini, A., Smiraglia, C., Diolaiuti, G., 2014. New data on glacier fluctuations during the climatic transition at ~4,000 cal. year BP from a buried log in the Forni glacier forefield (Italian Alps). Rend. Lincei. 25. https://doi.org/10.1007/s12210-014-0346-5.
Pintaldi, E., D'Amico, M.E., Colombo, N., Martinetto, E., Said-Pullicino, D., Giardino, M., Freppaz, M., 2021. Hidden paleosols on a high-elevation Alpine plateau (NW Italy): evidence for Lateglacial Nunatak? Glob. Planet. Chang. 207, 103676.
R Core Team, 2023. R: A Language and Environment for Statistical Computing. R Foundation for Statistical Computing, Vienna. https://www.R-project.org/.
Reimann, C., Filzmoser, P., Garrett, R.G., Dutter, R., 2008. Statistical Data Analysis Explained: Applied Environmental Statistics with RWiley, Chichester. ISBN: 978-0-470-98581-6.
Reimer, P.J., Austin, W.E.N., Bard, E., Bayliss, A., Blackwell, P.G., Bronk Ramsey, C., Butzin, M., Cheng, H., Edwards, R.L., Friedrich, M., Grootes, P.M., Guilderson, T.P., Hajdas, I., Heaton, T.J., Hogg, Konrad, A.G., Hughen, A., Kromer, B., Manning, S.W., Muscheler, R., Palmer, J.G., Pearson, C., van der Plicht, J., Reimer, R.W., Richards, D.A., Scott, E.M., Southon, J.R., Turney, C.S.M., Wacker, L., Adolphi, F., Büntgen, U., Capano, M., Fahrni, S.M., Fogtmann-Schulz, A., Friedrich, R., Köhler, P., Kudsk, S., Miyake, F., Olsen, J., Reinig, F., Sakamoto, M., Sookdeo, A., Talamo, S., 2020. The IntCal20 northern hemisphere radiocarbon age calibration curve (0–55 cal kBP). Radiocarbon 62 (4), 725–757. https://doi.org/10.1017/RDC.2020.41.
Rühland, K., Paterson, A.M., Smol, J.P., 2015. Lake diatom responses to warming: reviewing the evidence. J. Paleolimnol. 54 (1), 1–35.
Rull, V., 2008. Microrefugia. J. Biogeogr. https://doi.org/10.1111/j.1365-2699.2008.02023.x.
Scherrer, D., Körner, C., 2010. Infra-red thermometry of alpine landscapes challenges climatic warming projections. Glob. Chang. Biol. 16, 2602–2613.
Schmidt, R., Kamenik, C., Tessadri, R., Koinig, K.A., 2006. Climatic changes from 12,000 to 4,000 years ago in the Austrian Central Alps tracked by sedimentological and biological proxies of a lake sediment core. J. Paleolimnol. 35, 491–505.
Schönswetter, P., Stehlik, I., Holderegger, R., Tribsch, A., 2005. Molecular evidence for glacial refugia of mountain plants in the European Alps. Mol. Ecol. 14, 3547–3555. https://doi.org/10.1111/j.1365-294X.2005.02683.x.
Smith, B.N., Epstein, S., 1970. Biogeochemistry of the stable isotopes of hydrogen and carbon in salt marsh biota. Plant Physiol. 46 (5), 738–742.
Smol, J.P., Wolfe, A.P., Birks, H.J., Douglas, M.S., Jones, V.J., Korhola, A., Pienitz, R., Rühland, K., Sorvari, S., Antoniades, D., Brooks, S.J., Fallu, M.A., Hughes, M., Keatley, B.E., Laing, T.E., Michelutti, N., Nazarova, L., Nyman, M., Paterson, A.M., Perren, B., Quinlan, R., Rautio, M., Saulnier-Talbot, E., Siitonen, S., Solovieva, N., Weckström, J., 2005. Climate-driven regime shifts in the biological communities of arctic lakes. Proc. Natl. Acad. Sci. USA 102 (12), 4397–4402. https://doi.org/10.1073/pnas.0500245102. Mar 22.
Solovieva, N., Jones, V., Birks, J.H.B., Appleby, P., Nazarova, L., 2008. Diatom responses to 20th century climate warming in lakes from the northern Urals, Russia. Palaeogeogr. Palaeoclimatol. Palaeoecol. 259 (2–3), 96–106.
Stewart, J.R., Lister, A.M., 2001. Cryptic northern refugia and the origins of modern biota. Trends Ecol. Evol. 16, 608–613.
Stewart, J.R., Lister, A.M., Barnes, I., Dalén, L., 2010. Refugia revisited: individualistic responses of species in space and time. Proc. R. Soc. Lond. B Biol. Sci. 277 (1682), 661–671.
Strunk, A., Olsen, J., Sanei, H., Rudra, A., Larsen, N.K., 2020. Improving the reliability of bulk sediment radiocarbon dating. Quat. Sci. Rev. 242, 106442.
Tarca, G., Guglielmin, M., 2022. Evolution of the sparse debris cover during the ablation season at two small Alpine glaciers (Gran Zebrù and Sforzellina, Ortles-Cevedale group). Geomorphology 409, 108268.
Taylor, A.M., Brooks, J.R., Lachenbruch, B., Morrell, J.J., 1987. Radial patterns of carbon isotopes in the xylem extractives and cellulose of Douglas-fir. Tree Physiol. 27, 921–927.
Van Dam, H., Mertens, A., Sinkeldam, J., 1994. A coded checklist and ecological indicator values of freshwater diatoms from the Netherlands. Neth. J. Aquat. Ecol. 28, 117–133.
Van Geel, B., Buurman, J., Waterbolk, H.T., 1996. Archeological and paleoecological indications for an abrupt climate change in the Netherlands and evidence for climatological teleconnections around 2650 BP. J. Quat. Sci. 11 (6), 451–460.
Vyse, S.A., Herzshuh, U., Andreev, A.A., Pestryakova, L.A., Diekmann, B., Amitage, S.J., Biskaborn, B.K., 2020. Geochemical and sedimentological responses of arctic glacial Lake Ilirney, Chukotka (far East Russia) to palaeoenvironmental change since ~51.8 ka BP. Quat. Sci. Rev. 247, 106607.
Züllig, H., 1982. Untersuchungen über die Stratigraphie von Carotinoiden im geschichteten Sediment von 10 Schweizer Seen zur Erkundung früherer Phytoplankton-entfaltungen. Schweiz. Z. Hydrol. 44 (1), 1–98.